Title

Circularity in polydiketoenamine thermoplastics via control over reactive chain conformation.

Journal

Science Advances, 11(4)

Authors

Demarteau, Jeremy

Epstein, Alexander

Reed, Laura

et al.

Publication Date

2025-01-24

DOI

10.1126/sciadv.ads8444

Peer reviewed

CHEMISTRY

Circularity in polydiketoenamine thermoplastics via control over reactive chain conformation

Jeremy Demarteau[1], Alexander R. Epstein[2], Laura J. Reed[1], Nicodemo R. Ciccia[3,4], John F. Hartwig[3,4], Kristin A. Persson[1,2], Brett A. Helms[1,5,6]*

Controlling the reactivity of bonds along polymer chains enables both functionalization and deconstruction with relevance to chemical recycling and circularity. Because the substrate is a macromolecule, however, understanding the effects of chain conformation on the reactivity of polymer bonds emerges as important yet underexplored. Here, we show how oxy-functionalization of chemically recyclable condensation polymers affects acidolysis to monomers through control over distortion and interaction energies in the rate-limiting transition states. Oxy-functionalization of polydiketoenamines at specific sites on either the amine or triketone monomer segments increased acidolysis rates by more than three orders of magnitude, opening the door to efficient deconstruction of linear chain architectures. These insights substantially broaden the scope of applications for polydiketoenamines in a circular manufacturing economy, including chemically recyclable adhesives for a diverse range of surfaces.

INTRODUCTION

Encoding circularity in polymers is important for enabling and perfecting the chemical recycling of plastic waste (*1*–*4*). However, monomer-to-monomer circularity remains out of reach for the most widely used plastics, particularly polyethylene and polypropylene, due to their lack of readily cleavable bonds (*5*). Introducing heteroatoms as cleavage sites along polymer backbones has emerged as a versatile solution (*6*–*8*), reminiscent of how circularity is achieved with biopolymers in living systems (*9*, *10*). Yet, it remains unclear how the proximity of polar functionality near cleavage sites affects hydrolysis rates in an aqueous medium, where a diverse range of intermolecular interactions can alter reaction coordinates, polymer chain conformations, and energy landscapes governing the rate-limiting step. If this were understood, then it would be possible to deconstruct plastics to specific monomers or even oligomers at tunable fast rates.

Here, we show that oxy-functionalization of amine and triketone monomers at specific sites near acid-cleavable diketoenamine (DKE) bonds results in polydiketoenamine (PDK) deconstruction rates that are tunable more than three orders of magnitude (Fig. 1), enabling the creation of circular PDK thermoplastics and adhesives therefrom. To inform the basis by which oxy-functionalization might give rise to tunable deconstruction rates, we modeled the transition states for a series of oxy-functionalized DKE molecules and calculated the standard free energies of activation for hydrolysis, which differed by up to 20.6 kJ mol^{-1} due to structural changes between reactive conformations. To varying degrees by each DKE variant, an incoming water molecule could be guided to the iminium reaction center by hydrogen bonding, balancing energetic contributions for intermolecular interactions and intramolecular distortion, ultimately lowering free-energy barriers and increasing reaction rates. We synthesized the corresponding polymers and evaluated their deconstruction behaviors in strong aqueous acid. Most notably, in verifying the computational predictions, we also found that the extent of depolymerization to triketone and amine monomers was complete in preferred versatile designs, being informative for this emerging family of circular materials. We were also able to deconstruct PDK copolymers at specific sites, exploiting differences in hydrolysis rates for each comonomer. Encoding circularity in PDK through oxy-functionalization, optionally returning monomers or oligomers of defined length, is enabling in that chemical waste produced when recycling polymers is ultimately tied to the number of bonds breaking and reforming in the circular polymer lifecycle. We also find that oxy-functionalization improves the strength of PDK thermoplastics when they are used as hot-melt adhesives to a diverse range of substrates, particularly glass.

Our work lays a strong foundation for an expanded family of circular PDK thermoplastics to complement a growing number of chemically recyclable polymers that exploit heteroatoms to encode circularity (*6*–*8*, *11*–*42*). While remarkable insights into monomer designs have made it possible to controllably polymerize and depolymerize plastics along these lines, in this study we go further by highlighting the profound importance of remote substituent effects on the lability of cleavable bonds in condensation polymers via control over reactive chain conformations, which has largely been underexplored. From this vantage point, we achieved high rates, yields, and purities for the recovered monomers while also uncovering the design rules for circularity with both molecular and macromolecular precision.

RESULTS

Modeling hydrolysis rates of oxy-functionalized DKEs

Until now, circularity in PDK resins had been demonstrated for cross-linked thermosets, elastomers, and filled rubbers (*38*, *43*, *44*). To enable chemical recycling of thermoplastics, which are composed of linear chains, we hypothesized that the necessary low barrier to acidolysis might be achieved through oxy-functionalization of the diamine, which should pre-organize the transition state into a more favorable reactive conformation, while also increasing the activity of water through hydrogen bonding. We also considered

[1]The Molecular Foundry, Lawrence Berkeley National Laboratory, Berkeley, CA 94720, USA. [2]Department of Materials Sciences and Engineering, University of California, Berkeley, CA 94720, USA. [3]Department of Chemistry, University of California, Berkeley, Berkeley, CA 94720, USA. [4]Division of Chemical Sciences, Lawrence Berkeley National Laboratory, Berkeley, CA 94720, USA. [5]Materials Sciences Division, Lawrence Berkeley National Laboratory, Berkeley, CA 94720 USA. [6]Joint BioEnergy Institute, Emeryville, CA 94608, USA.
*Corresponding author. Email: bahelms@lbl.gov

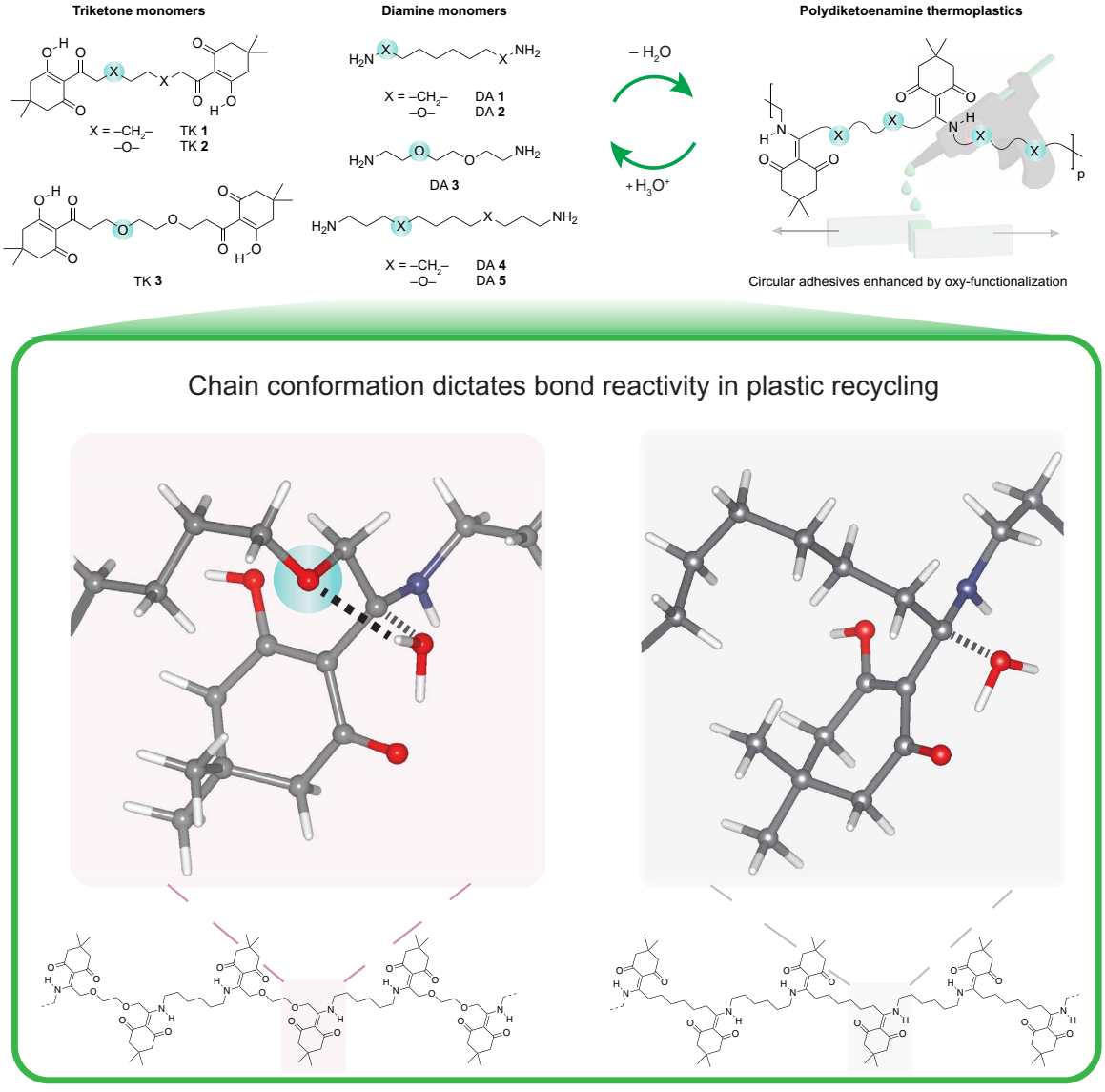

Fig. 1. Oxy-functionalization dictates reactive chain conformation and efficiency of circularity in recyclable polydiketoenamine thermoplastics. The efficiency by which linear polydiketoenamines (PDK) are deconstructed to triketone and amine monomers in acidolytic medium is both tunable and fast by controlling reactive chain conformation in oxy-functionalized PDK materials.

whether a similar effect might be achieved in oxy-functionalized triketone monomers, given the proximal relationship of those segments along the polymer chain. This latter approach would be particularly attractive in that the diamine monomer would no longer require oxy-functionalization. It would, therefore, become possible to use simpler diamines to formulate PDK thermoplastics with different properties without sacrificing circularity.

To test these hypotheses, we determined the ensemble of lowest energy structures of ionized iminium intermediates and their subsequent transition states during acidolysis for small-molecule DKEs, whose 1-hexylamine bonding partner featured either no oxy-functionalization (DKE **1**) or site-specific oxy-functionalization within one, two, three, or four conjoining bonds of the nitrogen (DKEs **2** to **5**, respectively). We generated these ensembles using the conformer-rotamer sampling tool (CREST) (*45*) and refined their free energies using hybrid density functional theory (DFT). We then calculated the hydrolysis reaction rate with multipath transition state theory (MP-TST) (fig. S1) (*44*, *46*, *47*) and examined the relative rates of acidolysis ($k/k_{control}$) for oxy-functionalized DKEs **2** to **5**, using the rate for unmodified DKE **1** as the control ($k_{control}$) (Fig. 2A). Through this analysis, we found that all oxy-functionalized derivatives delivered rate increases over an unmodified control concurrent with stabilizing hydrogen bonds between the sites of oxy-functionalization and the attacking water molecule. Yet, these rate increases were not uniform. The behavior overall was non-monotonic, with DKEs **3** and **4** delivering the highest rate increases by more than three orders of magnitude.

The computational modeling suggests that two competing factors contribute to the extent of stabilization: first, the distance (d) between the site of oxy-functionalization and the nearest hydrogen in the attacking water molecule, where stronger dispersion interactions led to

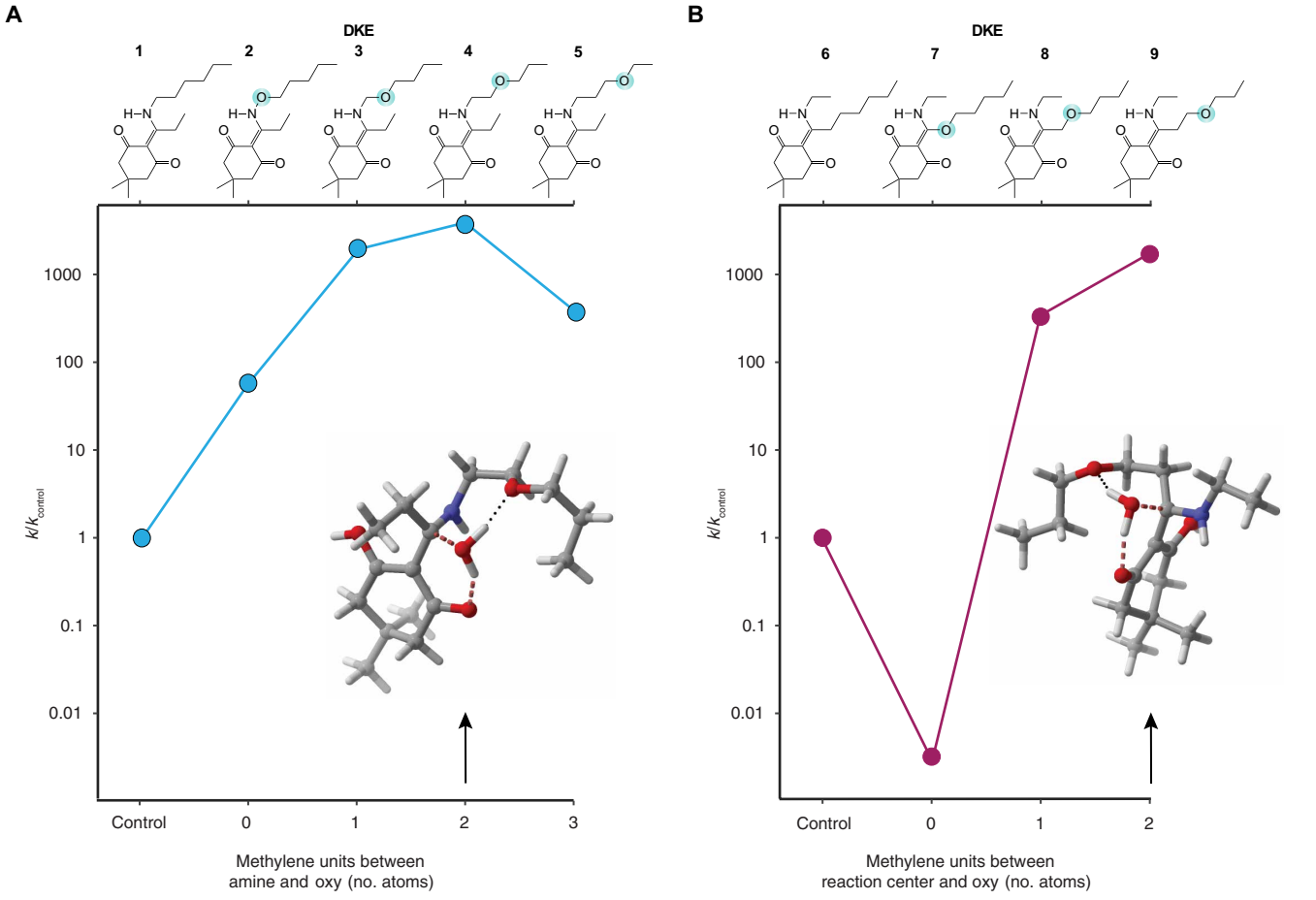

Fig. 2. Relative rates of hydrolysis for oxy-functionalized diketoenamine (DKEs). (**A**) Relative rates of hydrolysis for DKEs **1** to **5**, which are differentiated on the manner and placement of oxy-functionality in the amine coupling partner. Relative rates are normalized to DKE **1** as the control. (**B**) Relative rates of hydrolysis for DKEs **6** to **9**, which are differentiated on the manner and placement of oxy-functionality in the triketone coupling partner. Relative rates are normalized to DKE **6** as the control.

a shorter stronger bond; second, the torsion angle ϕ(C═C─C═N) of the iminium in its reactive conformation, where a larger torsion angle resulted in a larger energetic penalty to reach the lowest-energy transition state (fig. S2). We observed that, when no methylene unit was present between the amine and the site of oxy-functionalization (DKE **2**), the interatomic distance between the site of oxy-functionalization and the closest hydrogen atom in water was too long in the transition state to establish a hydrogen bond. As the number of methylene spacers between the site of oxy-functionalization and the reaction center increased, however, *d* decreased and plateaued at a length characteristic of a hydrogen bond, stabilizing the transition state. For DKE **4** and DKE **5**, the torsion angle required to achieve a hydrogen-bonded reactive configuration substantially increased. Thus, the energetic stabilization from the hydrogen bond is partially cancelled by the strain energy to achieve a reactive conformation. Therefore, there are optimal sites for oxy-functionality in DKE molecules (i.e., DKE **4**) and likely motifs in polymers based on them that balance stabilization and strain.

We performed the same sequence of calculations on DKEs **6** to **9**, where DKE **6** served as an unmodified control and DKEs **7** to **9** featured oxy-functionalization at progressively longer spacing along the triketone (Fig. 2B). We found that the highest rates of acidolysis were predicted for DKE **8** and DKE **9**. The reactive conformations in their lowest-energy transition states for DKEs **7** to **9** revealed a similar trend to that for DKEs **2** to **5**: DKE **9** forms a hydrogen bond with the attacking water, increasing the acidolysis rate, whereas DKE **7** and DKE **8** have weaker dispersion interactions (fig. S2). The most substantial difference from these trends was observed for DKE **7**, where the computed acidolysis rate is suppressed relative to the unmodified control. Here, oxy-functionalization directly affects the electronic structure at the reaction center. Further investigations, for example, using molecular dynamics, could elucidate polymer chain conformation beyond the small-molecule approximation but are outside the scope of this work.

To assess the validity of theoretical predictions that oxy-functionalization of amine and triketone monomers is poised to accelerate DKE hydrolysis rates, we synthesized from a selection of three triketones and five diamines (Fig. 3) a focused series of PDK resins **1** to **7** (Fig. 3A) via "click" polycondensation. This focus reflects a few key observations that we made during our investigations. We noted thermal instability of PDK materials generated using alkoxymethanamines, having similar structural characteristics to DKE **3**; bonding motifs of that type were, therefore, not carried forward. Likewise, we did not further explore PDK designs

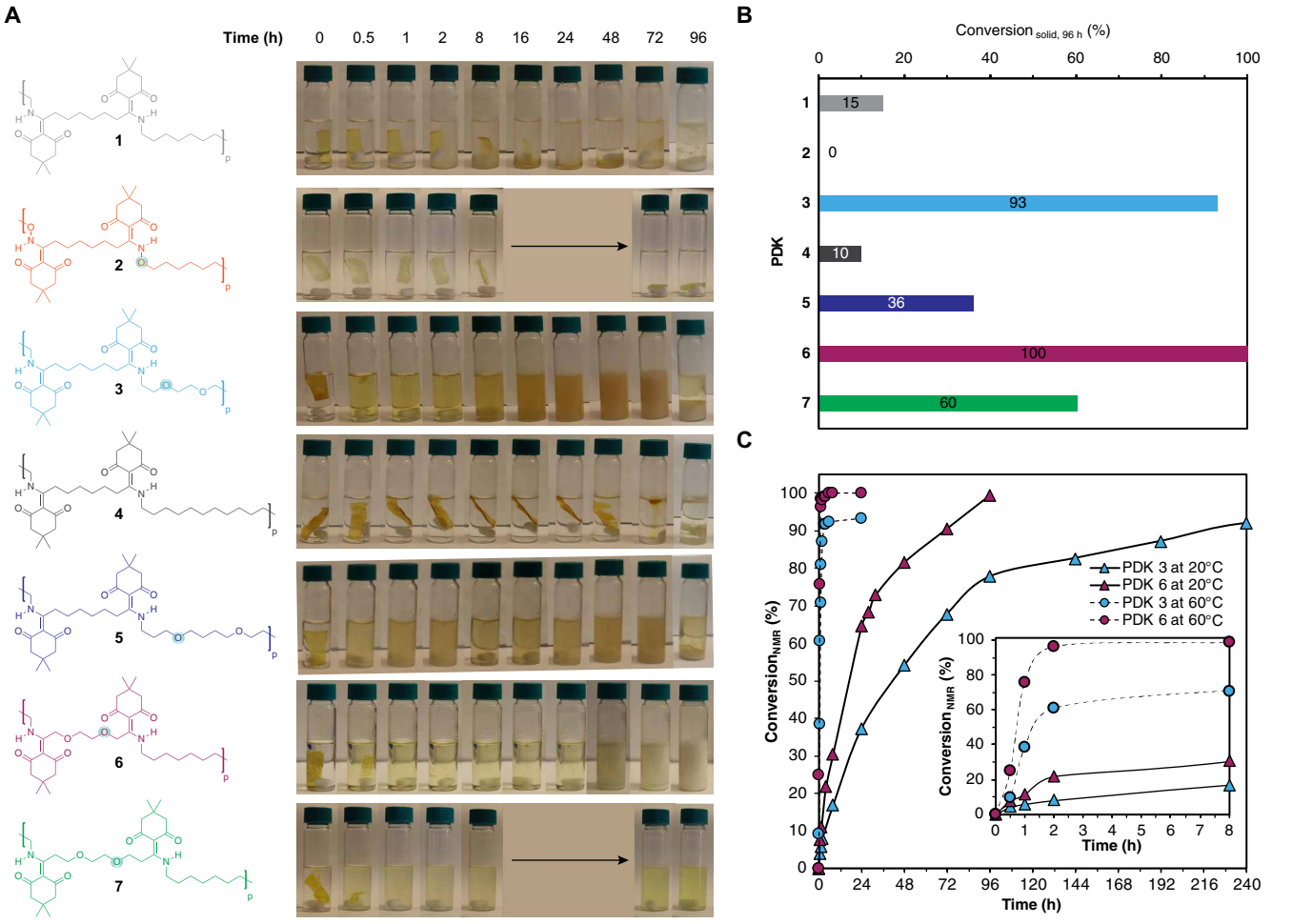

Fig. 3. Chemical recycling of PDK 1 to 7 thermoplastics in strong aqueous acid. (**A**) Visual progression of the depolymerization trajectory over time. (**B**) Conversion of PDK resins to monomer after 96 hours in 5.0 M HCl at 20°C. (**C**) Divergent conversion rates of oxy-functionalized PDKs **3** and **6** to monomer over time in 5.0 M HCl at either 20° or 60°C, showcasing the benefits of implementing oxy-functionalized triketone monomers to facilitate PDK deconstruction at the fastest rates in the highest yields at the lowest temperature. h, hours.

based on bonding motifs similar to DKE **7**, because those materials are known to undergo amine exchange twice, liberating the alcohol (*48*–*50*). This behavior does not permit retention of oxy-functionalization after polymerization; the hypothetical PDK hydrolysis behavior is, therefore, untestable. With these considerations as a guide, we synthesized PDKs **1** to **7** with weight-averaged molar masses (M_w) of 10 to 46 kg mol^{-1}. The synthesis of PDKs **6** and **7** resulted in the formation of oligomers, as shown in the SEC data (fig. S5), which were challenging to remove through precipitation. We also determined their glass transition temperatures (T_g) by differential scanning calorimetry and found that T_g values ranged from 16° to 63°C (table S1 and figs. S4 to S6). We could conduct the polymerization in solution or in polymer melts (fig. S3); however, we found that, for PDKs **2**, **6**, and **7**, addition of a solvent is beneficial, favoring higher degrees of polymerization (table S2 and fig. S7).

Verifying predictions for deconstruction of oxy-functionalized PDK thermoplastics

We observed the deconstruction behaviors of PDKs **1** to **7** in 5.0 M HCl at 20°C for 96 hours (Fig. 3A). With regard to changes in physical states of the polymers undergoing acidolysis and the accompanying monomers generated therefrom, there were notably different behaviors for the unmodified control compared to oxy-functionalized polymers. For PDK **1** and PDK **4**, which do not feature oxy-functionalization in either amine or triketone monomers, we observed a transition from a solid densified polymer sample suspended in the reaction medium to a viscous liquid, suggesting possible ionization, but little or no hydrolysis, i.e., the ionized polyelectrolyte served primarily as a viscosity modifier to the reaction medium. On the other hand, for oxy-functionalized PDK **3** and PDKs **5** to **7**, we observed that, after ionization and solubilization of polymer chains, the liberated triketones became apparent as dispersed solids in the reaction medium yet at different times for variants within the series. PDK **3** and PDK **6** stood out for their fast progression from dense solids to ionized and then soluble polymers undergoing hydrolysis; we observed dispersed triketone monomers after hydrolysis was complete.

In support of this interpretation of the visual progression, we confirmed by ^{1}H nuclear magnetic resonance (NMR) the chemical identities of the dispersed solids after filtration and drying as the original triketone monomers (figs. S8 and S9). For quantitative analysis of

PDK deconstruction behaviors, we calculated the percent conversion from recovered solids, taking account of the triketone-to-oligomer ratio from the accompanying ^{1}H NMR data (Fig. 3B and figs. S10 to S16); the chemical shift for hydrogen-bound O—H in the triketone monomer is at δ 17 to 19 parts per million (ppm), while that for the hydrogen-bound N—H in oligomeric DKEs is at δ 12 to 16 ppm.

We found that conversions for PDK **1** and PDK **4** bearing no oxy-functionalization were less than 16% by ^{1}H NMR, consistent with our predictions that acidolysis rates would be slow. On the other hand, PDK **3** containing oxy-functionalized amine monomers achieved 93% conversion, consistent with the theoretical prediction of a markedly faster rate. Increasing the number of methylenes between the DKE bond and the site of oxy-functionalization in the amine monomer led to a notable reduction in conversion as predicted, with PDK **5** achieving only 36% conversion after 96 hours. However, no deconstruction of PDK **2** occurred under these reaction conditions, deviating substantially with regard to theory. For PDK **6** and PDK **7** bearing oxy-functionality in the triketone (TK) monomer, we found conversions of 100 and 60%, respectively. While the structural integrity of recovered TK **2** monomer from PDK **6** was pristine after chemical recycling (fig. S15), TK **3** recovered from PDK **7** exhibited signs of chemical degradation due to retro-Michael reactions with the appearance of multiple peaks in the δ 17- to 19-ppm region (fig. S16). We further confirmed structural features in materials (monomers, oligomers, or polymers) recovered after hydrolysis to those of pristine PDK (i.e., before depolymerization) using matrix-assisted laser desorption/ionization (MALDI) time-of-flight mass spectrometry (figs. S17 to S23).

Even if deconstruction was relatively fast in the initial stages, depending on the site of oxy-functionalization within amine or triketone monomers, we recovered either exclusively the original triketone and amine monomers after acidolysis as desired or monomers contaminated with oligomeric impurities (figs. S10 to S14). To understand the implications of these behaviors at different reaction temperatures, we quantified the isolated monomer yields and monomer-to-oligomer ratios for PDK **3**, prepared with the fastest-to-deconstruct oxy-functionalized diamine monomer DA **3**, and PDK **6**, prepared with the fastest-to-deconstruct oxy-functionalized ditopic triketone monomer TK **2**. When deconstructed at ambient temperature, PDK **3** returned solids with an overall conversion of 71% yet a monomer-to-oligomer ratio of 93:7 (fig. S12). Increasing the temperature to 60°C resulted in a 99:1 monomer-to-oligomer ratio. Acidolysis of PDK **6**, on the other hand, gave an 86% isolated yield of monomer with no oligomer impurities (fig. S15). This is further corroborated by monitoring and tracking conversion, monomer:oligomer ratios, and isolated triketone yields for PDK **3** and PDK **6** deconstruction at either 20° or 60°C (Fig. 3C). At 20°C, PDK **6** achieved 90% conversion of DKE bonds to triketones within 72 hours; PDK **3** required 10 days to reach the same conversion. At 60°C, PDK **6** reached complete conversion in only 2 hours; PDK **3** reached 93% conversion after 24 hours.

In short, if the goal is to deconstruct PDK resins with linear topologies at the fastest possible rates with exclusive monomer recovery in high yield and high purity, then oxy-functionalization of amine monomers is preferred with two methylenes separating amine and ether functionalities. More preferred, however, is the oxy-functionalization of the triketone monomer with a single methylene spacer between the exocyclic ketone and ether functionalities. In support of this recommendation, acidolysis rates are substantially faster with PDK **6** (and likely variants thereof); monomers are recovered in the highest yield and purity; and, when practiced at scale, the shorter residence time in the reactor ultimately lowers the costs of chemical recycling (*51*, *52*).

We recognize that this recommendation will most likely appeal to those interested in recovering exclusively monomers when chemically recycling plastics. Nonetheless, this knowledgebase of polymer reactivity also suggests that it should be possible to control which bonds in PDK chains hydrolyze, e.g., through copolymers where oxy-functionalization is introduced at intervals determined by monomer placement within the chain, on the basis of the more favorable energetics associated with the reactive conformation of the polymer in acid. This is underexplored in synthetic polymers yet a natural consequence of requirements for transition-state pre-organization. In other words, oxy-functionalization encodes when and where the PDK chain is kinetically likely to cleave under experimentally accessible reactions conditions due to the effects of oxy-functionalization on the local chain conformation in acidolytic medium, rather than the intrinsic lability of the cleavable bond in the absence of oxy-functionalization.

Selective chain deconstruction in oxy-functionalized PDK copolymers

To demonstrate that PDK circularity is encodable via oxy-functionalization, we introduced oxy-functionalized TK **2** as a preferred cleavage site in otherwise slow-to-deconstruct PDK chains comprising TK **1** and DA **4** monomers (Fig. 4A); PDKs **8** to **11** comprising 0.02, 0.07, 0.24, and 0.37 equivalents of TK **2**, respectively, exhibited weight-averaged molar masses ranging from 85 to 158 kg mol^{-1} (fig. S24 and table S3). After deconstruction at 20°C in 5.0 M HCl (Fig. 4B), heteroatom-free PDK **8** exhibited minimal physical changes as expected, while PDK **11** with 37% oxy-functionalization in the triketone monomer feed lost its original shape and exhibited features reminiscent of a soft hydrogel. This is consistent with the expectation that deconstruction at the preferred sites produces oligomers of defined length, depending on extent of oxy-functionalization. To support this interpretation, we assessed the molar masses of the deconstructed PDKs **8** to **11** after deconstruction by size exclusion chromatography (SEC) (fig. S25 and table S3). We found that the ratio of final to initial molar masses scaled with the extent of oxy-functionalized TK **2** monomer in the feed ratio (Fig. 4C).

Oxy-functionalization enhances the adhesive properties of circular PDK thermoplastics

Considering the thermal properties of these PDK thermoplastics (T_g = 16° to 63°C), their adhesive properties may be of interest. Hot-melt adhesives typically comprise epoxies or polyurethanes, which struggle to close the loop in chemical recycling (*53*). As such, most complicate recycling efforts for materials in bonded assemblies, including aluminum, polymers, glass, and stainless steel. We bonded pairs of substrates taken from aluminum, nylon 6,6, glass, and stainless steel. As test cases, we initially used either heteroatom-free PDK **1** or oxy-functionalized PDK **3** (Fig. 5A and table S4) as the hot-melt adhesive. We identified glass substrates as having the best adhesive properties, with the lap shear strength averaging ~11.1 MPa for oxy-functionalized PDK **3**. Across all substrate types, oxy-functionalized PDK **3** consistently showed higher values compared to heteroatom-free PDK **1**, suggesting a general positive influence of oxy-functionalization on enhancing adhesive strength compared to its exact heteroatom-free analog.

To verify this hypothesis across the entire series, we performed tests for lap shear strength for pairs of glass substrates bonded

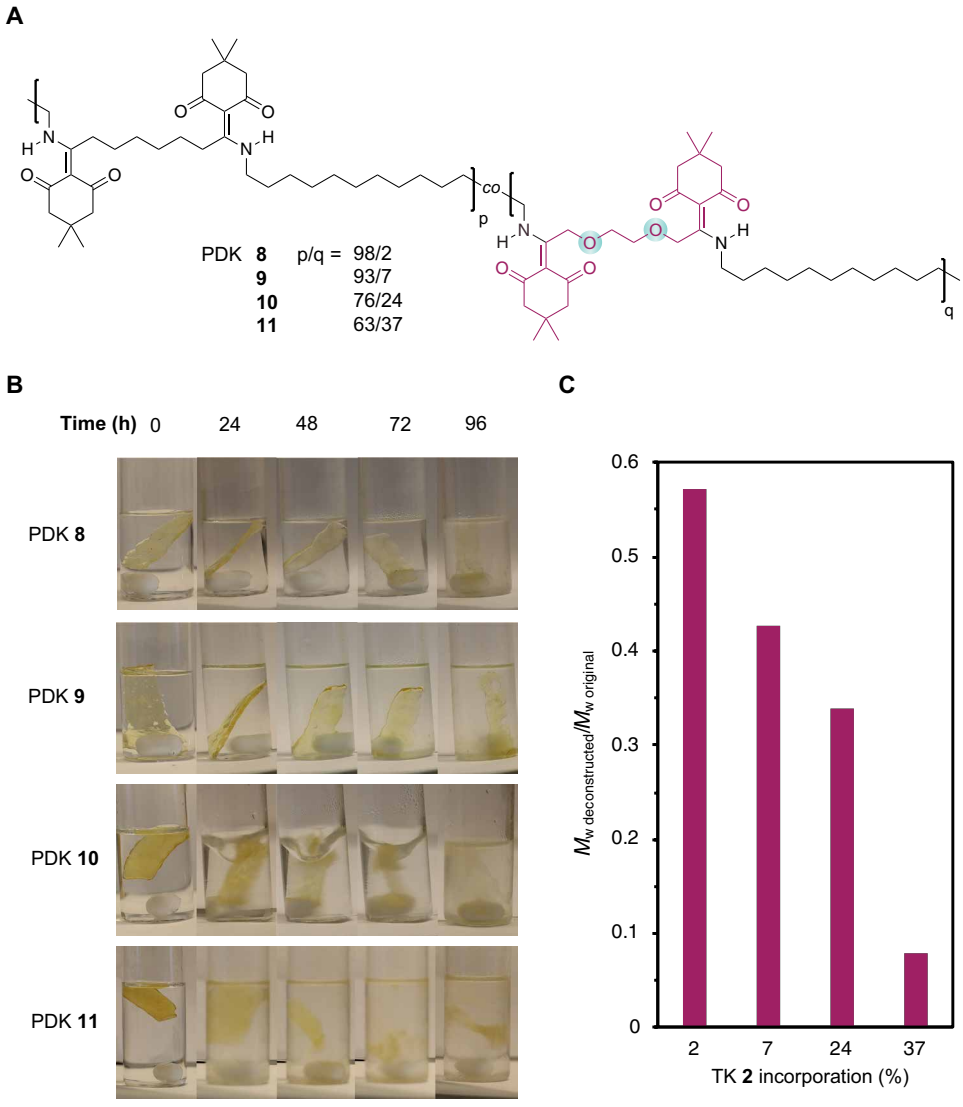

Fig. 4. Depolymerization of oxy-functionalized copolymers PDK 8 to 11 thermoplastics in strong aqueous acid. (**A**) The extent of oxy-functionalization was encoded by the relative amount of TKs **1** and **2** in the monomer feed alongside DA **4**. (**B**) Visual trajectory of the chemical depolymerization of PDKs **8** to **11** over time in 5.0 M HCl at 20°C. (**C**) Ratio of deconstructed molar mass to the initial molar mass of PDKs **8** to **11** as a function of TK **2** incorporation.

together by PDK adhesives. In standardized tests with adhesives configured with rectangular areas, lap shear tests of PDKs **3** to **6** consistently caused the bonded assemblies to fail due to excessive adhesive force (i.e., their lap shear strength was too high). We reduced the test area to 3- to 5-mm-diameter discs, which yielded testable specimens across all samples. PDKs **3** to **6** exhibited the highest lap shear strength values, where oxy-functionalized PDK **5** showed a value of 25.0 MPa (Fig. 5B and table S5). As reference points, commercially available adhesives, ethyl cyanoacrylate (Loctite Super Glue), epoxy (J-B Weld), and Gorilla Glue, have shown lap shear strength values ranging from 6.5 to 9.4 MPa on glass as a substrate (*53*). To quantify the benefits of oxy-functionalized PDK adhesives over their exact heteroatom-free counterparts, we calculated the lap shear strength ratios (Fig. 5C). Oxy-functionalized PDK **3** demonstrated hot-melt adhesive properties that are 4.5 times greater than their respective heteroatom-free counterpart; the adhesive strength of PDK **5** exceeds that of PDK **4**, although the difference is less pronounced compared to the ratios observed between PDKs **3** and **1** or between PDKs **6** and **1** (table S6). PDK **6** was 6.3 times stronger as an adhesive than the corresponding heteroatom-free PDK **1**.

DISCUSSION

Our findings demonstrate that polymer reactivity can be controlled by understanding how remote functionalization to cleavable bonds influences the energetics of transition states of bond cleavage from the perspective of their reactive chain conformation. These effects are exquisitely tunable, shown here via oxy-functionalization and rate acceleration in the deconstruction of PDKs, which is immediately relevant to plastics recycling and circularity. This includes the creation of circular adhesives, where oxy-functionalization produces more strongly bonded assemblies

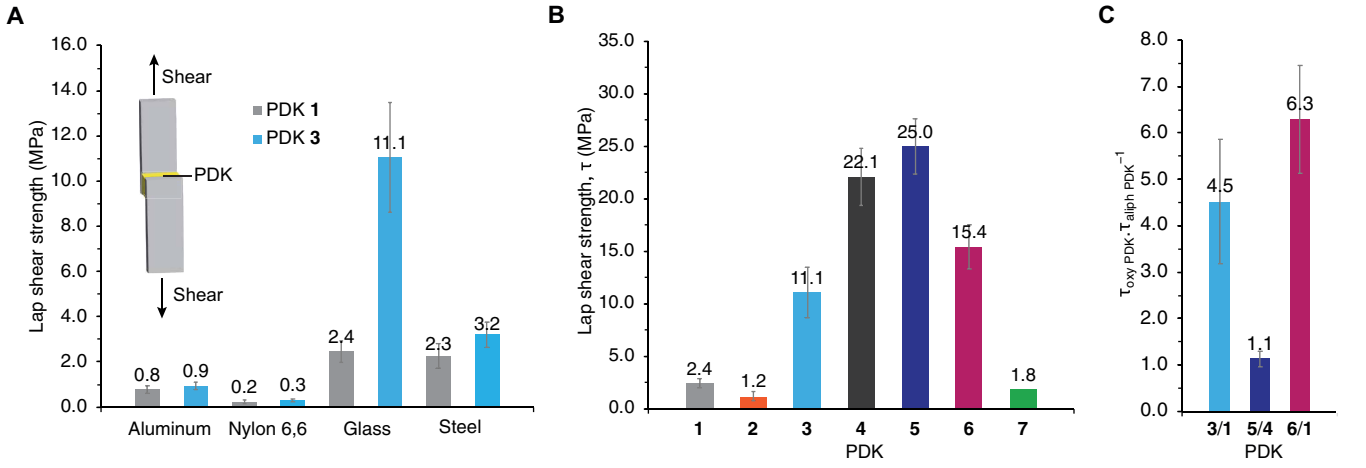

Fig. 5. Lap shear adhesion of polydiketoenamines (PDK) thermoplastics on different substrates. (**A**) Lap shear adhesion on aluminum, nylon-6,6, glass, and steel surfaces of PDKs **1** and **3**. (**B**) Lap shear adhesion of PDKs **1** to **7** on glass surfaces. (**C**) Ratio of lap shear strength of oxy-functionalized PDKs to their exact heteroatom-free counterparts. Error bars represent standard deviation from the mean taken from three independent tests.

of a diverse range of materials. From a broader perspective, the placement of heteroatoms in polymers appears to be a general strategy for promoting chain cleavage across natural and synthetic polymers, albeit with different mechanistic underpinnings, e.g., if deconstruction is spontaneous, promoted by an endogenous enzyme or an exogenous catalyst. Yet, in all these instances, reactive polymer chain conformation manifests as a guiding principle not often considered in polymer reactivity. Moreover, the implication that a synchronicity of non-covalent interactions is necessary to attain a reactive chain conformation suggests that polymer dynamics may also play an important role. From this vantage point, we see exciting opportunities to explore the macromolecular context underlying circularity principles for chemical and biological deconstruction of plastics with deep relevance to sustainability, environmental health, and the manufacturing economy.

MATERIALS AND METHODS

Materials

1,8-Diaminooctane (99%), 1,12-diaminododecane (98%), 2,2′-(ethylenedioxy)bis(ethylamine) (98%), 4,9-dioxa-1,12-dodecanediamine (99%), suberic acid (>98%), dodecanedioic diacid (99%), 5,5-dimethyl-1,3-cyclohexanedione (dimedone, 95%), *N*,*N*′-dicyclohexylcarbodiimide (99%), 4-(dimethylamino)pyridine (>99%), 1,6-dibromohexane (96%), *N*-hydroxyphthalimide (97%), 1,8-diazabicyclo[5.4.0]undec-7-ene (>99%), hydrazine monohydrate (N_2H_4, 64 to 65%; reagent grade, 98%), aluminum oxide (Al_2O_3), sodium trifluoroacetate (NaTFA, 99%), dithranol (99%), sodium sulfate (anhydrous, >99.5%), potassium hydroxide (KOH, 99%), and hydrochloric acid (HCl) were purchased from Sigma-Aldrich and used as received. 2,2′-[1,2-Ethanediylbis(oxy)]bis[acetic acid] (97%) was purchased from Ambeed and used as received. Bis-PEG2-acid was purchased from AccelaChem and used as received. All solvents—methanol (MeOH) (>99.9%), dimethylformamide (DMF) (>99.8%), ethanol (96%), cyclohexane (99%), hexane (99%), dichloromethane (DCM) (99%), acetone (99%), chloroform ($CHCl_3$) (>99%), and ethyl acetate (>99%)—were purchased from VWR and used without further purification.

Methods

NMR spectroscopy

^1H and ^{13}C NMR spectroscopy were carried out using a Bruker Avance II at 500 and 125 MHz, respectively. Chemical shifts are reported in δ (ppm) relative to the residual solvent peak, $CDCl_3$: 7.26 for ^1H and 77.16 for ^{13}C. Splitting patterns are designated as s (singlet), d (doublet), t (triplet), q (quartet), and m (multiplet).

Fourier transform infrared spectroscopy

Data were acquired using a Thermo-Fisher Nicolet iS50 spectrometer in attenuated total reflectance mode, as an average of 32 scans over 400 to 4000 cm^{-1}.

Size exclusion chromatography

SEC using DMF (containing 0.2% w/v LiBr) as the mobile phase was carried out using a customized system consisting of a Shimadzu LC-20 AD pump, Viscotek VE 3580 refractive index detector, and two mixed bed columns connected in series (Viscotek GMHHR-M). The system was operated at a temperature of 55°C and at 0.7 ml min^{-1}. Calibration on the system was performed using the refractive index increment (*dn*/*dc)* calculated from the measured refractive index values (with refractometer) at different concentrations.

SEC using THF as the mobile phase was performed on a Malvern OMNISEC equipped with refractive index, light scattering, and intrinsic viscosity detectors calibrated using a triple detection system. The system was operated at a temperature of 35°C and at 1 ml min^{-1}.

Differential scanning calorimetry

Data were acquired using a TA Instruments Q200 differential scanning calorimeter. Samples were heated over a temperature range of −50° to 250°C for PDKs **1**, **3**, **4**, and **5**; −50° to 120°C for PDKs **2**, **6**, and **7**, at a rate of 10°C min^{-1} for the heating step and 50°C min^{-1} for the cooling step under a N_2 atmosphere. For each sample, data acquisition runs consisted of a heating step, a cooling step, and a second heating step. Glass transition temperatures (T_g) were interpreted and reported from the second heating curve.

Thermogravimetric analysis

Thermogravimetric analysis (TGA) was performed on a TA Instruments TGA5500 thermal analyzer. First, samples were heated under nitrogen from 20° to 150°C and held at 150°C for 60 min. Then, the

samples were heated under nitrogen at a rate of 10°C min^{-1} from 20° to 800°C. Mass loss and degradation temperatures were interpreted and reported from the second heating ramp (20° to 800°C).

Matrix-assisted laser desorption/ionization time-of-flight mass spectrometry

MALDI mass spectra were recorded using a Bruker rapifleX spectrometer in positive reflector mode. A solution containing equivalent volume of analyte solution (1 mg ml^{-1} in CH_2Cl_2), matrix solution (dithranol, 10 mg ml^{-1} in CH_2Cl_2), and sodium trifluoroacetate solution (NaTFA, 1 mg ml^{-1} in CH_2Cl_2:MeOH 1:3 v:v) was prepared, and 1 μl of this mixture was applied to a stainless-steel target plate and allowed to dry completely before analysis.

Lap-shear tensile testing

Lap shear adhesion testing was conducted according to ASTM D1002-10 on an Instron universal materials tester equipped with a 1-kN load cell with a shear rate of 1.5 mm min^{-1}. Four types of substrates were used: aluminum, nylon 6,6, glass, and steel. Aluminum, nylon, and steel were each 0.16 to 0.4 cm thick by 1 cm wide by 10 cm long. For glass substrates, standardized rectangular area lap shear testing of PDKs **3** to **6** consistently led to the failure of the glass due to excessive adhesive force. Consequently, the testing area on glass substrates was reduced to 3- to 5-mm-diameter round-shaped adhesives to produce viable specimens. PDKs were applied as hot-melt adhesive using a hot plate (60°C) for 1 min to create a homogenous layer of the melted polymer on the lower substrate. Then, the sample was clamped with the upper substrate and thermally processed at elevated temperature in a convection oven (140°C for PDKs **1**, **3**, **4**, and **5**; 100°C for PDKs **2**, **6**, and **7**).

Shear strength was determined using the following equation below. The maximum force (F) was divided by the bonded area (A) covered by PDK, which was measured with digital calipers prior to testing

$$\text{Lap shear strength, } \tau \text{ (MPa)} = \frac{F\ (N)}{A\ (\text{mm}^2)}$$

Values in Fig. 5C were calculated using the equation of the independent quotient: $q = \frac{x}{y}$, where q corresponds to the PDK ratio and x and y correspond to the mean lap shear strength values of the corresponding PDK.

The uncertainty of the independent quotient was calculated as follows

$$\partial q = |q| \sqrt{\left(\frac{\partial x}{x}\right)^2 + \left(\frac{\partial y}{y}\right)^2}$$

Theoretical methods

Acidolysis rates were calculated using a MP-TST approach, where the multiple low-energy conformers are included in the total rate calculation (*46*)

$$k_{\text{MP-TST}} = \frac{k_B T}{h} \left(\frac{\sum_i^{\text{TS conf.}} e^{-\frac{\Delta E_i}{k_B T}} Q_{\text{TS},i}}{\sum_j^{\text{R conf.}} e^{-\frac{\Delta E_j}{k_B T}} Q_{\text{R},j}} \right) e^{-\frac{E_{\text{TS},0} - E_{\text{R},0}}{k_B T}}$$

Here, we first take the rate according to a single-structure energetic span approach

$$k = \frac{k_B T}{h} \frac{Q_{\text{TS}}}{Q_{\text{R}}} e^{-\frac{E_{\text{TS},0} - E_{\text{R},0}}{k_B T}}$$

where Q_{TS} and $E_{\text{TS},0}$ are the energy and partition functions of the lowest-energy transition state conformer, Q_{R} and $E_{\text{R},0}$ are the energy and partition functions of the lowest-energy reactant conformer, k_B is Boltzmann's constant, T is temperature, and h is Planck's constant. MP-TST then adjusts this single-structure by modifying the partition functions to be summed over all conformers of the transition state and reactant where each is weighted by its Boltzmann probability relative to the lowest-energy conformer. These terms are the partition function $Q_{\text{TS},i}$ and the energy difference ΔE_i for the ith transition state conformer and $Q_{\text{R},i}$ and ΔE_j for the jth reactant conformer. In this work, the number of conformers and the size of the molecule make the sum over all conformers computationally intractable. Instead, we used contributions from the lowest-energy conformers, which have previously been shown to yield accurate reaction rates for DKE acidolysis (*44*).

To identify the most important contributions to the MP-TST rate calculation, we used the following conformer searching workflow. First, a guess for a transition state structure for the addition of water for each DKE was taken from the acidolysis reaction pathway identified in previous work (*40*) and depicted for DKEs **1** to **9** in Fig. 2. The transition state was identified by optimization to a saddle point geometry at the wb97XD/6-311+G(d,p)/SMD level of theory (*54*, *55*). We then performed a conformer search using CREST to identify the ensemble of conformers with the lowest energy. CREST was run with constraints on the geometry local to the reaction center: the distance between the *O* nucleophile and the *C* electrophile and the distance between the *O* nucleophile and the H that dissociates to the cyclic ketone. For the 20 lowest-energy transition states, final transition state geometries were optimized at the wb97XD/6-311+G(d,p)/SMD level of theory. Reactants were then generated by perturbing transition state structures along the vibrational mode corresponding to the single imaginary frequency in the Hessian to generate reactants. In addition, CREST was run on the reactant structure, and the lowest-energy conformer from CREST was added to the reactant ensemble. Reactants were then also optimized at the wb97XD/6-311+G(d,p)/SMD level of theory. The free energy of the reactant was taken with the H_2O and DKE at infinite separation due to the variability in energies from small differences in the location of the single water molecule and the frequent failures in geometry optimization with one explicit water molecule. All hybrid-DFT calculations were performed using Gaussian 16 (*56*). The vibrational component of the partition function was calculated using the quasi-rigid rotor harmonic oscillator approximation for the vibrational entropy (*57*).

To assess the impact of only including 20 conformers in the MP-TST rate calculation, fig. S1 depicts the convergence of the MP-TST as a function of the number of transition state conformers included. The rate is depicted below as a rate relative to the control, which contains no oxy-functionality, as differentiation of DKE acidolysis rates is of primary interest here rather than quantitative precision in the absolute rate. As the number of conformers included in the MP-TST rate calculation increases, the relative rate is affected, but by less than an order of magnitude. In general, this does not change the qualitative ordering of acidolysis rates as a function of oxy spacing. However, the corrections are quite important in identifying the

decrease in rate observed for an amine-oxy spacing of three methylene units.

Acid-catalyzed hydrolytic depolymerization of thermoplastic PDK

General procedure. Thermoplastic PDK (~500 mg) were each placed in a 20-ml vial containing strong acid (5.0 M HCl, 15 ml) and a magnetic stirrer. Depolymerization reactions were conducted at either 20° or 60°C at different time points.

Quantitative recovery. Hydrolysis reactions for yield determination were stopped at determined time points. The mixture was centrifuged, and the liquid was separated from the solid. This step was repeated twice with fresh portions of HCl (5.0 M, 15 ml), followed by two successive centrifugations of the solid with fresh portions of deionized water (15 ml).

NMR kinetics. Hydrolysis kinetics were proceeded by sampling out aliquots (50 to 100 μl) of the reaction mixture, which were then transferred into separate NMR tubes for extraction of the soluble monomer in $CDCl_3$, seeking ^1H NMR analysis and conversion determination.

Supplementary Materials

The PDF file includes:

Supplementary Text
Figs. S1 to S25
Tables S1 to S6
Legend for data S1
References

Other Supplementary Material for this manuscript includes the following:

Data S1

REFERENCES AND NOTES

1. C. Jehanno, J. W. Alty, M. Roosen, S. De Meester, A. P. Dove, E. Y.-X. Chen, F. A. Leibfarth, H. Sardon, Critical advances and future opportunities in upcycling commodity polymers. *Nature* **603**, 803–814 (2022).
2. G. W. Coates, Y. D. Y. L. Getzler, Chemical recycling to monomer for an ideal, circular polymer economy. *Nat. Rev. Mater.* **5**, 501–516 (2020).
3. L. T. J. Korley, T. H. Epps, B. A. Helms, A. J. Ryan, Toward polymer upcycling-adding value and tackling circularity. *Science* **373**, 66–69 (2021).
4. L. D. Ellis, N. A. Rorrer, K. P. Sullivan, M. Otto, J. E. McGeehan, Y. Román-Leshkov, N. Wierckx, G. T. Beckham, Chemical and biological catalysis for plastics recycling and upcycling. *Nat. Catal.* **4**, 539–556 (2021).
5. S. T. Schwab, M. Baur, T. F. Nelson, S. Mecking, Synthesis and deconstruction of polyethylene-type materials. *Chem. Rev.* **124**, 2327–2351 (2024).
6. M. Häußler, M. Eck, D. Rothauer, S. Mecking, Closed-loop recycling of polyethylene-like materials. *Nature* **590**, 423–427 (2021).
7. M. Eck, S. T. Schwab, T. F. Nelson, K. Wurst, S. Iberl, D. Schleheck, C. Link, G. Battagliarin, S. Mecking, Biodegradable high-density polyethylene-like material. *Angew Chemie Int. Ed.* **62**, e202213438 (2023).
8. B. A. Abel, R. L. Snyder, G. W. Coates, Chemically recyclable thermoplastics from reversible-deactivation polymerization of cyclic acetals. *Science* **373**, 783–789 (2021).
9. V. V. Andhalkar, R. Ahorsu, P. Domínguez de María, J. Winterburn, F. Medina, M. Constantí, Valorization of lignocellulose by producing polyhydroxyalkanoates under circular bioeconomy premises: Facts and challenges. *ACS Sustain. Chem. Eng.* **10**, 16459–16475 (2022).
10. K. A. Fransen, S. H. M. Av-Ron, T. R. Buchanan, D. J. Walsh, D. T. Rota, L. Van Note, B. D. Olsen, High-throughput experimentation for discovery of biodegradable polyesters. *Proc. Natl. Acad. Sci. U.S.A.* **120**, e2220021120 (2023).
11. Y.-J. Jang, S. Nguyen, M. A. Hillmyer, Chemically recyclable linear and branched polyethylenes synthesized from stoichiometrically self-balanced telechelic polyethylenes. *J. Am. Chem. Soc.* **146**, 4771–4782 (2024).
12. X.-T. Wu, C. Yang, J.-S. Xi, C. Shi, F.-S. Du, Z.-C. Li, Enabling closed-loop circularity of "non-polymerizable" α, β-conjugated lactone towards high-performance polyester with the assistance of cyclopentadiene. *Angew. Chemie Int. Ed.* **63**, e202404179 (2024).
13. M. Birkle, H. S. Mehringer, T. F. Nelson, S. Mecking, Aliphatic polyester materials from renewable 2,3-butanediol. *ACS Sustain. Chem. Eng.* **12**, 4156–4163 (2024).
14. T. F. Nelson, D. Rothauer, M. Sander, S. Mecking, Degradable and recyclable polyesters from multiple chain length bio- and waste-sourceable monomers. *Angew. Chemie Int. Ed.* **62**, e202310729 (2023).
15. J.-B. Zhu, E. M. Watson, J. Tang, E. Y.-X. Chen, A synthetic polymer system with repeatable chemical recyclability. *Science* **360**, 398–403 (2018).
16. X. Tang, E. Y.-X. Chen, Toward infinitely recyclable plastics derived from renewable cyclic esters. *Chem* **5**, 284–312 (2019).
17. A. Sangroniz, J.-B. Zhu, X. Tang, A. Etxeberria, E. Y.-X. Chen, H. Sardon, Packaging materials with desired mechanical and barrier properties and full chemical recyclability. *Nat. Commun.* **10**, 3559 (2019).
18. X.-L. Li, R. W. Clarke, J.-Y. Jiang, T.-Q. Xu, E. Y.-X. Chen, A circular polyester platform based on simple gem-disubstituted valerolactones. *Nat. Chem.* **15**, 278–285 (2023).
19. C. Shi, N. A. Rorrer, A. L. Shaw, R. W. Clarke, B. L. Buss, G. T. Beckham, L. J. Broadbelt, E. Y.-X. Chen, Topology-accelerated and selective cascade depolymerization of architecturally complex polyesters. *J. Am. Chem. Soc.* **146**, 9261–9271 (2024).
20. X.-W. Han, X. Zhang, Y. Zhou, A. Maimaitiming, X.-L. Sun, Y. Gao, P. Li, B. Zhu, E. Y.-X. Chen, X. Kuang, Y. Tang, Circular olefin copolymers made de novo from ethylene and α-olefins. *Nat. Commun.* **15**, 1462 (2024).
21. C. Shi, M. L. McGraw, Z.-C. Li, L. Cavallo, L. Falivene, E. Y.-X. Chen, High-performance pan-tactic polythioesters with intrinsic crystallinity and chemical recyclability. *Sci. Adv.* **6**, eabc0495 (2020).
22. L. Zhou, L. T. Reilly, C. Shi, E. C. Quinn, E. Y.-X. Chen, Proton-triggered topological transformation in superbase-mediated selective polymerization enables access to ultrahigh-molar-mass cyclic polymers. *Nat. Chem.* **16**, 1357–1365 (2024).
23. J. Yuan, W. Xiong, X. Zhou, Y. Zhang, D. Shi, Z. Li, H. Lu, 4-Hydroxyproline-derived sustainable polythioesters: Controlled ring-opening polymerization, complete recyclability, and facile functionalization. *J. Am. Chem. Soc.* **141**, 4928–4935 (2019).
24. D. J. Saxon, E. A. Gormong, V. M. Shah, T. M. Reineke, Rapid synthesis of chemically recyclable polycarbonates from renewable feedstocks. *ACS Macro Lett.* **10**, 98–103 (2021).
25. D. H. Lamparelli, A. Villar-Yanez, L. Dittrich, J. Rintjema, F. Bravo, C. Bo, A. W. Kleij, Bicyclic guanidine promoted mechanistically divergent depolymerization and recycling of a biobased polycarbonate. *Angew. Chemie Int. Ed. Engl.* **62**, e202314659 (2023).
26. T. M. McGuire, A. C. Deacy, A. Buchard, C. K. Williams, Solid-state chemical recycling of polycarbonates to epoxides and carbon dioxide using a heterodinuclear Mg(II)Co(II) catalyst. *J. Am. Chem. Soc.* **144**, 18444–18449 (2022).
27. G. Rosetto, F. Vidal, T. M. McGuire, R. W. F. Kerr, C. K. Williams, High molar mass polycarbonates as closed-loop recyclable thermoplastics. *J. Am. Chem. Soc.* **146**, 8381–8393 (2024).
28. J.-Z. Zhao, T.-J. Yue, B.-H. Ren, X.-B. Lu, W.-M. Ren, Closed-loop recycling of sulfur-rich polymers with tunable properties spanning thermoplastics, elastomers, and vitrimers. *Nat. Commun.* **15**, 3002 (2024).
29. T.-G. Hsu, S. Liu, X. Guan, S. Yoon, J. Zhou, W.-Y. Chen, S. Gaire, J. Seylar, H. Chen, Z. Wang, J. Rivera, L. Wu, C. J. Ziegler, R. McKenzie, J. Wang, Mechanochemically accessing a challenging-to-synthesize depolymerizable polymer. *Nat. Commun.* **14**, 225 (2023).
30. Y.-L. Su, L. Yue, H. Tran, M. Xu, A. Engler, R. Ramprasad, H. J. Qi, W. R. Gutekunst, Chemically recyclable polymer system based on nucleophilic aromatic ring-opening polymerization. *J. Am. Chem. Soc.* **145**, 13950–13956 (2023).
31. Y. Liu, Y. Jia, Q. Wu, J. S. Moore, Architecture-controlled ring-opening polymerization for dynamic covalent poly(disulfide)s. *J. Am. Chem. Soc.* **141**, 17075–17080 (2019).
32. Q. Zhang, Y. Deng, C.-Y. Shi, B. L. Feringa, H. Tian, D.-H. Qu, Dual closed-loop chemical recycling of synthetic polymers by intrinsically reconfigurable poly(disulfides). *Matter* **4**, 1352–1364 (2021).
33. T. O. Machado, C. J. Stubbs, V. Chiaradia, M. A. Alraddadi, A. Brandolese, J. C. Worch, A. P. Dove, A renewably sourced, circular photopolymer resin for additive manufacturing. *Nature* **629**, 1069–1074 (2024).
34. L. P. Manker, M. A. Hedou, C. Broggi, M. J. Jones, K. Kortsen, K. Puvanenthiran, Y. Kupper, H. Frauenrath, F. Marechal, V. Michaud, R. Marti, M. P. Shaver, J. S. Luterbacher, Performance polyamides built on a sustainable carbohydrate core. *Nat. Sustain.* **7**, 640–651 (2024).
35. R. M. Cywar, N. A. Rorrer, H. B. Mayes, A. K. Maurya, C. J. Tassone, G. T. Beckham, E. Y.-X. Chen, Redesigned hybrid nylons with optical clarity and chemical recyclability. *J. Am. Chem. Soc.* **144**, 5366–5376 (2022).
36. J.-J. Tian, X. Liu, L. Ye, Z. Zhang, E. C. Quinn, C. Shi, L. J. Broadbelt, T. J. Marks, E. Y.-X. Chen, Redesigned nylon 6 variants with enhanced recyclability, ductility, and transparency. *Angew. Chemie Int. Ed. Engl.* **63**, e202320214 (2024).
37. C. Shi, L. T. Reilly, V. S. Phani Kumar, M. W. Coile, S. R. Nicholson, L. J. Broadbelt, G. T. Beckham, E. Y.-X. Chen, Design principles for intrinsically circular polymers with tunable properties. *Chem* **7**, 2896–2912 (2021).
38. P. R. Christensen, A. M. Scheuermann, K. E. Loeffler, B. A. Helms, Closed-loop recycling of plastics enabled by dynamic covalent diketoenamine bonds. *Nat. Chem.* **11**, 442–448 (2019).
39. C. He, P. R. Christensen, T. J. Seguin, E. A. Dailing, B. M. Wood, R. K. Walde, K. A. Persson, T. P. Russell, B. A. Helms, Conformational entropy as a means to control the behavior of poly(diketoenamine) vitrimers in and out of equilibrium. *Angew. Chemie Int. Ed. Engl.* **59**, 735–739 (2020).

40. J. Demarteau, A. R. Epstein, P. R. Christensen, M. Abubekerov, H. Wang, S. J. Teat, T. J. Seguin, C. W. Chan, C. D. Scown, T. P. Russell, J. D. Keasling, K. A. Persson, B. A. Helms, Circularity in mixed-plastic chemical recycling enabled by variable rates of polydiketoenamine hydrolysis. *Sci. Adv.* **8**, eabp8823 (2022).
41. B. A. Helms, Polydiketoenamines for a circular plastics economy. *Acc. Chem. Res.* **55**, 2753–2765 (2022).
42. J. Demarteau, B. Cousineau, Z. Wang, B. Bose, S. Cheong, G. Lan, N. R. Baral, S. J. Teat, C. D. Scown, J. D. Keasling, B. A. Helms, Biorenewable and circular polydiketoenamine plastics. *Nat. Sustain.* **6**, 1426–1435 (2023).
43. E. A. Dailing, P. Khanal, A. R. Epstein, J. Demarteau, K. A. Persson, B. A. Helms, Circular polydiketoenamine elastomers with exceptional creep resistance via multivalent cross-linker design. *ACS Cent. Sci.* **10**, 54–64 (2024).
44. A. R. Epstein, J. Demarteau, B. A. Helms, K. A. Persson, Variable amine spacing determines depolymerization rate in polydiketoenamines. *J. Am. Chem. Soc.* **145**, 8082–8089 (2023).
45. P. Pracht, F. Bohle, S. Grimme, Automated exploration of the low-energy chemical space with fast quantum chemical methods. *Phys. Chem. Chem. Phys.* **22**, 7169–7192 (2020).
46. K. H. Møller, R. V. Otkjær, N. Hyttinen, T. Kurtén, H. G. Kjaergaard, Cost-effective implementation of multiconformer transition state theory for peroxy radical hydrogen shift reactions. *J. Phys. Chem. A* **120**, 10072–10087 (2016).
47. J. L. Bao, D. G. Truhlar, Variational transition state theory: Theoretical framework and recent developments. *Chem. Soc. Rev.* **46**, 7548–7596 (2017).
48. K. L. Diehl, I. V. Kolesnichenko, S. A. Robotham, J. L. Bachman, Y. Zhong, J. S. Brodbelt, E. V. Anslyn, Click and chemically triggered declick reactions through reversible amine and thiol coupling via a conjugate acceptor. *Nat. Chem.* **8**, 968–973 (2016).
49. G. J. Davis, H. A. Sofka, J. C. Jewett, Highly stable Meldrum's acid derivatives for irreversible aqueous covalent modification of amines. *Org. Lett.* **22**, 2626–2629 (2020).
50. V. Zhang, J. V. Accardo, I. Kevlishvili, E. F. Woods, S. J. Chapman, C. T. Eckdahl, C. L. Stern, H. J. Kulik, J. A. Kalow, Tailoring dynamic hydrogels by controlling associative exchange rates. *Chem* **9**, 2298–2317 (2023).
51. N. Vora, P. R. Christensen, J. Demarteau, N. R. Baral, J. D. Keasling, B. A. Helms, C. D. Scown, Leveling the cost and carbon footprint of circular polymers that are chemically recycled to monomer. *Sci. Adv.* **7**, eabf0187 (2022).
52. J. Demarteau, N. Vora, J. D. Keasling, B. A. Helms, C. D. Scown, Lower-cost, lower-carbon production of circular polydiketoenamine plastics. *ACS Sustain. Chem. Eng.* **10**, 2740–2749 (2022).
53. A. M. Rahman, C. Bowland, S. Ge, S. R. Acharya, S. Kim, V. R. Cooper, X. C. Chen, S. Irle, A. P. Sokolov, A. Savara, T. Saito, Design of tough adhesive from commodity thermoplastics through dynamic crosslinking. *Sci. Adv.* **7**, eabk2451 (2021).
54. A. V. Marenich, C. J. Cramer, D. G. Truhlar, Universal solvation model based on solute electron density and on a continuum model of the solvent defined by the bulk dielectric constant and atomic surface tensions. *J. Phys. Chem. B* **113**, 6378–6396 (2009).
55. J.-D. Chai, M. Head-Gordon, Long-range corrected hybrid density functionals with damped atom–atom dispersion corrections. *Phys. Chem. Chem. Phys.* **10**, 6615–6620 (2008).
56. M. J. Frisch, G. W. Trucks, H. B. Schlegel, G. E. Scuseria, M. a. Robb, J. R. Cheeseman, G. Scalmani, V. Barone, G. a. Petersson, H. Nakatsuji, X. Li, M. Caricato, a. V. Marenich, J. Bloino, B. G. Janesko, R. Gomperts, B. Mennucci, H. P. Hratchian, J. V. Ortiz, a. F. Izmaylov, J. L. Sonnenberg, Williams, F. Ding, F. Lipparini, F. Egidi, J. Goings, B. Peng, A. Petrone, T. Henderson, D. Ranasinghe, V. G. Zakrzewski, J. Gao, N. Rega, G. Zheng, W. Liang, M. Hada, M. Ehara, K. Toyota, R. Fukuda, J. Hasegawa, M. Ishida, T. Nakajima, Y. Honda, O. Kitao, H. Nakai, T. Vreven, K. Throssell, J. a. Montgomery Jr., J. E. Peralta, F. Ogliaro, M. J. Bearpark, J. J. Heyd, E. N. Brothers, K. N. Kudin, V. N. Staroverov, T. a. Keith, R. Kobayashi, J. Normand, K. Raghavachari, a. P. Rendell, J. C. Burant, S. S. Iyengar, J. Tomasi, M. Cossi, J. M. Millam, M. Klene, C. Adamo, R. Cammi, J. W. Ochterski, R. L. Martin, K. Morokuma, O. Farkas, J. B. Foresman, D. J. Fox, Gaussian 16 Revision C.01, Gaussian, Inc., Wallingford, CT (2016).
57. S. Grimme, Supramolecular binding thermodynamics by dispersion-corrected density functional theory. *Chemistry* **18**, 9955–9964 (2012).
58. N. Kuhl, M. Abend, S. Bode, U. S. Schubert, M. D. Hager, Oxime crosslinked polymer networks: Is every reversible covalent bond suitable to create self-healing polymers? *J. Appl. Polym. Sci.* **133**, 44168 (2016).

Acknowledgments

Funding: This work was funded by the US Department of Energy, Office of Science, Office of Basic Energy Sciences, Materials Sciences and Engineering Division under contract no. DE-AC02-05-CH11231 Unlocking Chemical Circularity in Recycling by Controlling Polymer Reactivity Across Scales program CUP-LBL-Helms. Data for this study were produced using computational resources provided by the Eagle HPC systems at the National Renewable Energy Laboratory (NREL), the Lawrencium HPC cluster at Lawrence Berkeley National Laboratory, and the Savio computational cluster resource provided by the Berkeley Research Computing program at the University of California, Berkeley (supported by the UC Berkeley Chancellor, Vice Chancellor for Research, and Chief Information Officer). A.R.E. was supported by the National Science Foundation Graduate Research Fellowship under grant no. DGE 1752814. Portions of this work, including PDK synthesis, characterization, and deconstruction, were carried out as a User Project at the Molecular Foundry, which is supported by the Office of Science and Office of Basic Energy Sciences of the US DOE under contract no. DE-AC02-05-CH11231. **Author contributions:** B.A.H. directed the study, and B.A.H. and J.D. designed the experiments and wrote the manuscript. J.D. and L.J.R. synthesized and characterized the monomers and polymers, processed the polymers, and conducted the kinetics experiments. J.D. performed macromolecular and thermomechanical characterization, conducted the recycling experiments, and conducted the lap shear adhesion testing. N.R.C. and J.F.H. designed the lap shear adhesion testing. K.A.P. directed and K.A.P. and A.R.E. designed and executed the computational studies. All coauthors participated in data analysis and interpretation. **Competing interests:** B.A.H. is an inventor on the US provisional patent application 62/587,148 (filed 16 November 2017), and B.A.H., A.R.E., J.D., and K.A.P. are inventors on US provisional patent application 63/390,962 (filed 20 July 2023), both submitted by Lawrence Berkeley National Laboratory that covers PDKs, as well as aspects of their use and recovery. B.A.H. has a financial interest in Cyklos Materials and Sepion Technologies. The other authors declare that they have no competing interests. **Data and materials availability:** All data needed to evaluate the conclusions in the paper are present in the paper and/or the Supplementary Materials. *XYZ* coordinates for the structures used in the computational study can be found at https://doi.org/10.5061/dryad.nk98sf835.

Submitted 30 August 2024
Accepted 19 December 2024
Published 22 January 2025
10.1126/sciadv.ads8444